

## RESEARCH ARTICLE

# Master–Slave Architecture Enhanced and Improved GBO Tuned Cascaded PI-PDN Controller for Speed Regulation of DC Motors

Davut Izci<sup>1,2,3</sup>  | Serdar Ekinci<sup>4</sup> | Rizk M. Rizk-Allah<sup>5,6</sup> | Nada Ibrahim Alribdi<sup>7</sup> | Aseel Smerat<sup>8,9,10</sup> | Ahmed Alzahrani<sup>11</sup> | Ayed Alwadain<sup>11</sup> | Vaclav Snasel<sup>6</sup>  | Laith Abualigah<sup>11</sup> 

<sup>1</sup>Department of Electrical and Electronics Engineering, Bursa Uludag University, Bursa, Turkey | <sup>2</sup>Applied Science Research Center, Applied Science Private University, Amman, Jordan | <sup>3</sup>Jadara University Research Center, Jadara University, Irbid, Jordan | <sup>4</sup>Department of Computer Engineering, Istanbul Gedik University, Istanbul, Turkey | <sup>5</sup>Basic Engineering Science Department, Faculty of Engineering, Menoufia University, Shebin El-Kom, Egypt | <sup>6</sup>Faculty of Electrical Engineering and Computer Science, VŠB-Technical University of Ostrava, Poruba-Ostrava, Czech Republic | <sup>7</sup>Department of Teaching and Learning, College of Education and Development, Princess Nourah Bint Abdulrahman University, Riyadh, Saudi Arabia | <sup>8</sup>Faculty of Educational Sciences, Al-Ahliyya Amman University, Amman, Jordan | <sup>9</sup>Centre for Research Impact & Outcome, Chitkara University Institute of Engineering and Technology, Chitkara University, Rajpura, Punjab, India | <sup>10</sup>Computer Technologies Engineering, Mazaya University College, Nasiriyah, Iraq | <sup>11</sup>Computer Science Department, Community College, King Saud University, Riyadh, Saudi Arabia

**Correspondence:** Laith Abualigah ([aligah.2020@gmail.com](mailto:aligah.2020@gmail.com))

**Received:** 2 November 2024 | **Revised:** 24 April 2025 | **Accepted:** 28 April 2025

**Funding:** This work was supported by Princess Nourah Bint Abdulrahman University Researchers Supporting Project number (PNURSP2025R594), Princess Nourah Bint Abdulrahman University, Riyadh, Saudi Arabia and European Union under the REFRESH—Research Excellence For REgion Sustainability and High-tech Industries project number CZ.10.03.01/00/22\_/0000048.

**Keywords:** adaptive local search mechanism | cascaded PI-PDN controller | DC motor speed management | experience-based perturbed learning strategy | gradient-based optimizer | stability

## ABSTRACT

This study introduces a novel master–slave architecture featuring an improved gradient-based optimizer (ImGBO) to effectively tune a cascaded proportional-integral (PI) and proportional-derivative with filter (PDN) controller specifically for DC motor speed regulation. The core novelty of this work lies in enhancing the traditional GBO algorithm by integrating an experience-based perturbed learning mechanism and an adaptive local search strategy, significantly enhancing its ability to balance exploration and exploitation during optimization. The proposed ImGBO-based cascaded PI-PDN controller is comprehensively evaluated against traditional GBO, recent metaheuristics and advanced proportional-integral-derivative (PID) and fractional-order PID (FOPID) controllers. Significant improvements were observed, with the proposed method demonstrating exceptionally short rise (0.0089 s) and settling times (0.0140 s), no overshoot, and minimal steady-state error (0.0017%). Stability analysis via pole placement and Bode plots affirmed the robust and stable operation of the controller, exhibiting a phase margin of 71.6640° and infinite gain margin. These results strongly support the suitability and effectiveness of the ImGBO-based approach for precision-critical DC motor control applications.

## 1 | Introduction

### 1.1 | Background

Direct current (DC) motors have been indispensable components in various industrial and engineering applications, extensively utilized where precise speed control and dynamic responsiveness are paramount. Due to their advantageous characteristics, such as excellent controllability, linear torque-speed profiles, and straightforward control schemes, DC motors remain pivotal in automation, robotics, electric vehicles, and numerous other applications demanding high accuracy and reliability [1, 2]. However, precise speed regulation of DC motors under varying loads and operating conditions remains a challenging problem. Traditional control approaches, such as conventional proportional-integral-derivative (PID) controllers [3], have long been employed due to their simplicity and ease of implementation. Nonetheless, these conventional methods often struggle to deliver the desired robustness and stability, especially under fluctuating operational conditions and parameter uncertainties [4]. Therefore, contemporary research is increasingly focused on developing advanced and robust control techniques, aiming to significantly enhance DC motor control performance by minimizing overshoot, reducing steady-state error, and improving dynamic responsiveness [5, 6].

Among the modern control strategies, cascaded controllers have gained substantial interest [7]. Cascaded architectures can improve system response by effectively managing disturbances, suppressing noise, and maintaining high dynamic stability, thereby offering considerable advantages over traditional PID and fractional order PID (FOPID) schemes [8–15]. Despite these benefits, optimal tuning of cascaded controllers poses substantial complexities, requiring advanced optimization techniques capable of systematically exploring large parameter spaces to identify optimal solutions [16]. Metaheuristic optimization algorithms have emerged as powerful tools to address this challenge, demonstrating significant potential in achieving precise parameter tuning for advanced control architectures [17–22].

### 1.2 | Related Works

In recent literature, various approaches have been investigated to enhance DC motor speed control. Traditional control methods, such as PID controllers, have been widely optimized using metaheuristics, demonstrating improved performance. For instance, Puangdownreong [4] applied the cuckoo search algorithm to optimize PID parameters, effectively achieving robust speed control with good tracking accuracy. Guo and Mohamed [5] presented an adaptive neuro-fuzzy inference system-based hybrid PID controller, significantly enhancing the motor's dynamic performance by reducing steady-state error and overshoot.

Recently, FOPID controllers have also received notable attention due to their additional tuning flexibility through fractional calculus. Izci et al. [6] optimized a fractional-order PID controller using an improved slime mold algorithm, demonstrating superior transient response and improved robustness compared to conventional PID controllers. Similarly, Zare et al. [9] proposed an optimal fractional-order tilt integral derivative (FOTID) controller,

achieving notable improvements in both stability and dynamic performance metrics of DC motor speed control systems.

Alternative robust control schemes, such as sliding-mode control, have been explored by researchers like Chen and Kuo [2], who designed a double-integral sliding-mode controller achieving robust and rapid response characteristics for brushless DC motor control. Advanced fuzzy logic controllers integrated with metaheuristics have also been proposed; Subramani et al. [17] introduced an improved African buffalo optimization-based Takagi-Sugeno-Kang fuzzy proportional-integral (PI) controller, significantly enhancing the motor's dynamic performance and reliability. Akbari-Hasanjani et al. [11] earlier provided insights into fuzzy PID controllers demonstrating the adaptability and improved control precision when encountering varying operational conditions.

Novel optimization algorithms are continuously introduced to enhance DC motor control further. Jabari et al. [7] recently utilized a multi-stage fractional-order PD (1+PI) controller optimized via the pelican optimization algorithm, resulting in improved transient performance, significantly reduced settling time, and lower steady-state errors. Similarly, Ayinla et al. [23] effectively implemented the leader-based Harris hawks optimization algorithm, demonstrating considerable enhancement in robustness and system response accuracy for DC motor speed control. Furthermore, recent advancements by Ekinci et al. [3] included a comprehensive comparative study on mountain gazelle optimizer for DC motors, validating superior control performance in challenging scenarios. Güven et al. [24] also demonstrated robust results utilizing a modified jellyfish search algorithm, optimizing PID controller parameters to significantly enhance control reliability and accuracy.

Additionally, nonlinearity-focused approaches were explored by Çelik et al. [25], who designed a nonlinear PI controller offering improved speed regulation capabilities by effectively handling nonlinearities inherent in PMDC motor drives. Despite these extensive contributions, challenges such as balancing exploration and exploitation in the optimization process, avoiding premature convergence, and achieving optimal parameter tuning in complex controller structures still require further investigation. Consequently, the continued development and refinement of robust and efficient control and optimization methods remain a priority research direction [26–28].

### 1.3 | Motivation

Despite substantial advancements in DC motor speed control achieved through various classical and advanced methods, achieving an optimal balance between robustness, precision, and dynamic responsiveness continues to be challenging [29–31]. Conventional control schemes such as PID and even advanced fractional-order PID controllers, while widely utilized, often suffer from performance limitations when subjected to varying operational conditions, including load fluctuations and external disturbances. Additionally, ensuring a proper balance between global exploration and local exploitation remains problematic in traditional optimization strategies, often leading to

premature convergence or suboptimal solutions. These limitations motivate the current study, focusing specifically on overcoming the inherent challenges in parameter optimization for cascaded proportional-integral (PI) and proportional-derivative (PDN) controllers. This work aims to address the existing gaps by introducing an enhanced gradient-based optimization approach (ImGBO) that leverages experience-based perturbed learning and adaptive local search mechanisms. Such enhancements aim not only to effectively avoid premature convergence but also to deliver a highly balanced search strategy, significantly improving control precision and robustness. The pursuit of these goals aligns closely with the practical demands of industries and applications that require exceptional accuracy, rapid response times, and stable motor control under varying operational scenarios.

## 1.4 | Contribution

The primary contributions and novelties of this study can be summarized as follows:

- A novel metaheuristic optimization algorithm, termed ImGBO, is introduced. It integrates two innovative strategies—experience-based perturbed learning (EPL) and adaptive local search (ALS), significantly enhancing exploration and exploitation capabilities. This improvement addresses common optimization challenges such as premature convergence and local optima entrapment, thereby yielding more accurate and reliable control solutions.
- A unique master–slave architecture utilizing Bode’s ideal reference model as the master system and the cascaded PI-PDN controller tuned by ImGBO as the slave system is presented. This framework ensures precise conformity to predefined dynamic performance specifications, enabling robust and stable regulation of DC motor speed.
- Extensive comparative studies validate the effectiveness of the proposed ImGBO-based cascaded PI-PDN controller against traditional gradient-based optimizer (GBO) and contemporary metaheuristics, including flood algorithm (FLA), RIME optimizer, and artificial hummingbird algorithm (AHA). Furthermore, rigorous comparisons with recent PID and FOPID-based controllers reported in the literature are conducted, providing a holistic evaluation of the proposed method’s relative advantages.
- The simulation results demonstrate notable improvements in critical performance metrics. Specifically, the ImGBO-based cascaded PI-PDN controller achieves exceptionally rapid rise (0.0089 s) and settling times (0.0140 s), zero overshoot, and minimal steady-state error (0.0017%), significantly surpassing the performance metrics reported by recently documented PID and FOPID-based controllers.
- The robustness and reliability of the proposed method are thoroughly verified via stability analyses utilizing pole placement and Bode plots. The analyses confirm the superior stability characteristics of the proposed control scheme, characterized by a high phase margin (71.6640°) and infinite gain margin, highlighting its suitability for precision-critical applications.

Collectively, these contributions underscore the significant advancements offered by the proposed ImGBO-based cascaded PI-PDN controller, providing a reliable, efficient, and practically viable solution for advanced DC motor speed control applications.

## 1.5 | Organization

The remainder of this manuscript is structured as follows. Section 2 provides the detailed mathematical modeling of the DC motor speed control system employed in the study, establishing the theoretical foundation required for controller development. Section 3 introduces the original GBO algorithm and thoroughly explains the proposed ImGBO, detailing its novel EPL and ALS components. Section 4 presents the maiden application of the proposed master–slave framework incorporating the ImGBO-tuned cascaded PI-PDN controller, clearly outlining the methodology, optimization constraints, and implementation strategy. Section 5 comprehensively discusses simulation results, including detailed comparisons with recent metaheuristic algorithms and statistical validations. Time-domain analyses, controller effort evaluations, and extensive comparative studies against state-of-the-art PID and FOPID controllers are included. Stability analyses employing pole placement and Bode plots further substantiate the robustness of the proposed control solution. Finally, Section 6 concludes the paper by summarizing key findings and contributions, underscoring the practical implications and effectiveness of the proposed approach, and providing recommendations for future research directions.

## 2 | Modeling of DC Motor Speed Control System

This work employs an externally excited DC motor, where speed control can be achieved by adjusting the armature voltage or current. The simplified block diagram for the DC motor drive is illustrated in Figure 1. The open loop transfer function describing the motor’s speed response to armature voltage is derived as follows. First, for a constant flux condition, the induced voltage  $e_b(t)$  is proportional to the rotational speed  $\omega(t)$  and is expressed as [32–34]:

$$e_b(t) = K_b \frac{d\theta(t)}{dt} = K_b \omega(t) \quad (1)$$

With an armature-controlled DC motor, the applied voltage  $e_a(t)$  must overcome both armature circuit drop and back emf:

$$e_a(t) = L_a \frac{di_a(t)}{dt} + R_a i_a(t) + e_b(t) \quad (2)$$

Assuming no external load, the armature current  $i_a(t)$  generates the torque required to overcome inertia and friction. Hence:

$$T(t) = J \frac{d\omega(t)}{dt} + B\omega(t) = K_m i_a(t) \quad (3)$$

where  $J$  is the moment of inertia,  $B$  is the friction constant, and  $K_m$  is the motor torque constant. Taking the Laplace transform with zero initial conditions yields:

$$E_b(s) = K_b \Omega(s) \quad (4)$$

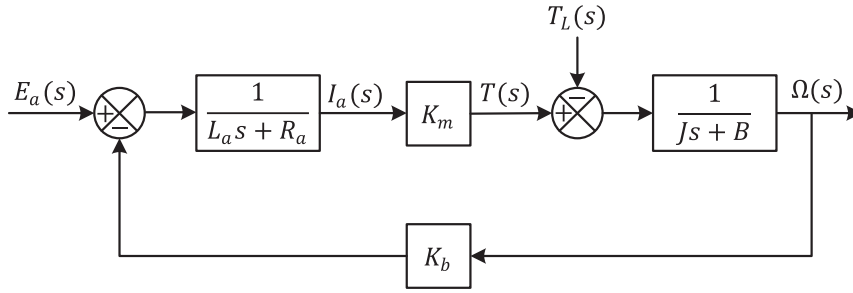


**FIGURE 1** | Block diagram of DC motor speed system.

$$E_a(s) = (L_a s + R_a) I_a(s) + E_b(s) \quad (5)$$

$$T(s) = (J s + B) \Omega(s) = K_m I_a(s) \quad (6)$$

Eliminating  $I_a(s)$  to relate the output speed  $\Omega(s)$  to the input voltage  $E_a(s)$  gives the open loop transfer function:

$$G_P(s) = \frac{\Omega(s)}{E_a(s)} = \frac{K_m}{(L_a s + R_a)(J s + B) + K_b K_m} \quad (7)$$

In keeping with parameters reported in [35, 36], the DC motor is assigned:  $R_a = 0.4 \Omega$ , armature inductance  $L_a = 2.7 \text{ H}$ ,  $J = 4 \times 10^{-4} \text{ kg m}^2$ ,  $B = 2.2 \times 10^{-3} \text{ N m s/rad}$ ,  $K_m = 1.5 \times 10^{-2} \text{ N m/A}$ , and electromotive force constant  $K_b = 5 \times 10^{-2} \text{ V s/rad}$ . Substituting these values into Equation (7) yields the open-loop plant of  $G_P(s) = 0.015 / (0.00108s^2 + 0.0061s + 0.00163)$ .

### 3 | Gradient-Based Optimizer and Its Improved Version

Gradient-based optimization (GBO) is a metaheuristic approach inspired by Newton's rules and utilizes gradient-related concepts to tackle complex optimization problems [37]. GBO balances exploration and exploitation through two main operators: the gradient searching rule (GSR) and the local escaping operator (LEO). GSR expands the search domain to avoid premature convergence, while LEO refines promising solutions. The algorithm starts by randomly initializing a population of candidate solutions ( $Z_n$ ), ensuring diversity in the search space. Each solution is generated as follows:

$$Z_n = Z_{min} + rand \times (Z_{max} - Z_{min}), n = 1, 2, \dots, N \quad (8)$$

where  $N$  is the population size,  $rand$  is a random vector in  $[0, 1]$ , and  $Z_{min}$  and  $Z_{max}$  are the lower and upper boundaries of the search domain, respectively. GSR is designed to broaden exploration and reduce the likelihood of stagnation in local optima. It updates each solution  $Z_n^t$  in iteration  $t$  using a numerical gradient concept and direction of movement (DM). The GSR update is given by:

$$Z_n^{t+1} = Z_n^t - randn \times B_1 \times \frac{2\Delta Z \cdot Z_n^t}{(Z_{worst}^t - Z_{best}^t + \epsilon)} + rand \times B_2 \times (Z_{best}^t - Z_n^t) \quad (9)$$

where  $Z_{best}$  and  $Z_{worst}$  denote the current best and worst solutions, respectively,  $\epsilon \in [0, 0.1]$  is a small number,  $randn$  is drawn from a normal distribution, while  $rand$  is uniformly distributed in  $[0, 1]$ . The parameters  $B_1 = 2 \cdot rand \cdot a - a$  and  $B_2 = 2 \cdot rand \cdot a - a$  regulate exploration and exploitation where  $a$  and  $G$  have the following definitions.

$$a = \left| G \cdot \sin\left(\frac{3\pi}{2}\right) + \sin\left(G \cdot \frac{3\pi}{2}\right) \right| \quad (10)$$

$$G = 0.2 + \left(1 - \left(\frac{t}{T}\right)^3\right)^2 \quad (11)$$

Besides,  $\Delta Z = rand(1 : D) \cdot |step|$ , where:

$$step = \frac{(Z_{best}^t - Z_{r1}^t) + \gamma}{2} \quad (12)$$

$$\gamma = 2 \cdot rand \cdot \left( \left| \frac{Z_{r1}^t + Z_{r2}^t + Z_{r3}^t + Z_{r4}^t}{4} - Z_n^t \right| \right) \quad (13)$$

Here,  $r1, r2, r3, r4$  are distinct indices in the population ( $r1 \neq r2 \neq r3 \neq r4 \neq n$ ),  $D$  is the dimension of the solution,  $T$  is the maximum iteration count, and  $\Delta Z$  scales the movement step. A second updated solution  $Z2_n^t$  is formed by using  $Z_{best}$  in place of  $Z_n^t$ :

$$Z2_n^t = Z_{best} - randn \times B_1 \times \frac{2\Delta Z \cdot Z_n^t}{(yp_n^m - yq_n^m + \epsilon)} + rand \times B_2 \times (Z_{r1}^t - Z_{r2}^t) \quad (14)$$

where  $yp_n = rand \cdot (([Y_n^t + Z_n^t] / 2) + rand \cdot \Delta Z)$  and  $yq_n = rand \cdot (([Y_n^t + Z_n^t] / 2) - rand \cdot \Delta Z)$ . Here,  $Y_n^t$  is the previous iteration's solution. A "flag" mechanism then decides whether  $Y_n^t$  becomes  $Z1_n^t$  or  $Z2_n^t$ . To balance local and global exploration, the final solution for iteration  $t + 1$  is updated as:

$$Z_n^{t+1} = r_a \times (r_b \times Z1_n^t + (1 - r_b) \times Z2_n^t) + (1 - r_a) \times Z3_n^t \quad (15)$$

$$Z3_n^m = Z_n^t - \rho_1 \times (Z2_n^t - Z1_n^t) \quad (16)$$

The LEO stage boosts exploitation by combining multiple solution vectors. If  $rand < pr$ , LEO produces a new candidate  $Z_{LEO}^t$  via:

if  $rand < pr$

if  $rand < 0.5$

$$Z_{LEO}^t = Z_n^{t+1} + f_1 \times (v_1 \times Z_{best} - v_2 \times Z_k^t) + f_2 \times B_1 \times (v_3 \times (Z2_n^t - Z1_n^t) + v_2 \times (Z_{r1}^t - Z_{r2}^t)) / 2$$

$$Z_n^{t+1} = Z_{LEO}^t$$

else

$$Z_{LEO}^t = Z_{best} + f_1 \times (v_1 \times Z_{best} - v_2 \times Z_k^t) + f_2 \times \rho_1 \times (v_3 \times (Z2_n^t - Z1_n^t) + v_2 \times (Z_{r1}^t - Z_{r2}^t)) / 2$$

$$Z_n^{t+1} = Z_{LEO}^t$$

end

end

(17)

Here,  $f_1$  is uniformly distributed in  $[-1, 1]$ ,  $f_2$  follows a standard normal distribution, and  $pr$  is the switching probability. The coefficients  $v_1$ ,  $v_2$ , and  $v_3$  are computed as  $v_1 = H_1 \times 2 \times rand + (1 - H_1)$ ,  $v_2 = H_1 \times rand + (1 - H_1)$  and  $v_3 = H_1 \times rand + (1 - H_1)$  where  $H_1 \in \{0, 1\}$  is determined by a comparison of a uniform random  $v_1 \in [0, 1]$  with 0.5. Additionally,  $Z_k^m$  is updated as:

$$Z_k^m = H_2 \times Z_p^t + (1 - H_2) \times Z_{rand} \quad (18)$$

where  $Z_p^t$  is any randomly chosen solution from the population,  $Z_{rand} = Z_{min} + rand(0, 1) \times (Z_{max} - Z_{min})$ , and  $H_2 \in \{0, 1\}$  depends on another random threshold  $v_2 \in [0, 1]$ . By iteratively applying GSR and LEO, GBO adaptively balances global exploration with local refinement, demonstrating robust performance in locating high-quality solutions.

Although GBO demonstrates promising performance, it can still experience premature convergence and difficulties in maintaining a proper balance between exploration and exploitation in complex search spaces. In response, we propose an enhanced variant called ImGBO, which incorporates two major enhancements: experience-based perturbed learning (EPL) and an adaptive local search (ALS) mechanism [38]. EPL expands the exploration capability by guiding new candidate solutions toward promising regions, while ALS strengthens exploitation by refining the quality of solutions through collaborative updates among elite individuals.

The EPL component aims to broaden the search space by perturbed sampling around the current best solution ( $z_{best}$ ). For a randomly selected solution  $z_I^{it}$ , EPL computes the mean and deviation relative to  $z_{best}$ , then generates a new candidate ( $z_{new}^{it}$ ) accordingly. The procedure is given by:

$$\Delta_{mean}^{it} = (z_{best} + z_I^{it})/2 \quad (19)$$

$$\Delta_{dev}^{it} = \text{abs}(z_{best} - z_I^{it}) \quad (20)$$

$$\Delta_C^{it} = \Delta_{mean}^{it} + rand_1 \cdot \Delta_{dev}^{it} \quad (21)$$

$$\begin{aligned} z_{new}^{it} &= \Delta_C^{it} + rand_2 \cdot (z_{best} - \Delta_C^{it}) \\ &\quad + 0.95^{it} \cdot (rand_3 - 0.5) \cdot \text{abs}(z_{max,j} - z_{min,j}), z_{max,j} \\ &= \max_j \{z_I^{it}\}, z_{min,j} = \min_j \{z_I^{it}\} \forall \end{aligned} \quad (22)$$

Here,  $\Delta_{mean}^{it}$  and  $\Delta_{dev}^{it}$  capture the midpoint and absolute gap between  $z_{best}$  and the random solution  $z_I^{it}$ . The variables  $rand_1$ ,  $rand_2$ ,  $rand_3 \in [0, 1]$  are drawn from a uniform distribution, and the final term in Equation (22) introduces a perturbation whose range is adaptively updated ( $\Delta_{max}$  and  $\Delta_{min}$ ) over iterations. To mitigate performance deterioration during later stages and further refine high-quality areas, ImGBO integrates an ALS phase that shares information among an elite group. The method identifies each member's best ( $z^P$ ) and worst ( $z^W$ ) solutions, as well as the global best  $z_{best}$ . ALS then updates the worst candidate ( $z^W$ ) by attempting three possible movements in succession: (1) moving  $z^W$  toward  $z^P$ ; (2) moving  $z^W$  toward  $z_{best}$ ; and (3) moving  $z^W$  toward the midpoint ( $(z^P + z_{best})/2$ ). The procedure stops as soon as any of these movements yields improvement. Formally,

if  $z_I^{it}$  is the current worst candidate in the elite group, its updated solution  $z_I^{(it+1)}$  follows:

$$z_I^{it+1} = \begin{cases} z_1^{ALS} = 2 \times r_1 \times (z^P - z^W) + z^W & \text{if } f(z_1^{ALS}) \leq f(z_I^{it}) \\ z_2^{ALS} = 2 \times r_2 \times (z_{best} - z^W) + z^W & \text{else if } f(z_2^{ALS}) \leq f(z_I^{it}) \\ z_3^{ALS} = 2 \times r_3 \times ((z^P + z_{best})/2 - z^W) + z^W & \text{otherwise} \end{cases} \quad (23)$$

where  $r_1, r_2, r_3 \in [0, 1]$  are random scaling parameters and  $f$  is the objective (fitness) function. This adaptive updating scheme drives poor solutions toward promising directions, thereby improving the overall quality of the population. Figure 2 illustrates the overall flow of the proposed ImGBO, showing the seamless integration of EPL for exploration and ALS for exploitation.

## 4 | Maiden Application of a Novel Control Method for DC Motor Speed Regulation

### 4.1 | Cascaded PI-PDN Controller

The proposed cascaded PI-PDN controller unites two primary components [39], one based on proportional-integral (PI) control and the other on proportional-derivative with a filter (PDN), to deliver improved speed regulation for the DC motor. As depicted in Figure 3, this arrangement processes the motor's feedback signal in two sequential stages.

The PI stage, given in Equation (24) applies proportional ( $K_P$ ) and integral ( $K_I$ ) actions to address steady-state error and maintain robust low-frequency response.

$$C_{PI}(s) = K_P + \frac{K_I}{s} \quad (24)$$

The second stage (PDN) builds upon a proportional-derivative scheme, with an additional filter term governed by the coefficient  $N$  [40]. Equation (25) shows how the proportional gain ( $K_{PP}$ ) and the derivative gain ( $K_D$ ) integrate with the filter  $N$ , enhancing transient performance and mitigating noise susceptibility.

$$C_{PDN}(s) = K_{PP} + K_D \frac{Ns}{s + N} \quad (25)$$

Combining these two blocks results in the cascaded PI-PDN controller, expressed by Equation (26) [41].

$$C_{PI-PDN}(s) = \left( K_P + \frac{K_I}{s} \right) \left( K_{PP} + K_D \frac{Ns}{s + N} \right) \quad (26)$$

When this unified controller is paired with the DC motor plant  $G_P(s)$  from Equation (7) under unity feedback, the resulting closed-loop system can be represented by Equation (27). This final expression captures how the PI and PDN components act jointly to minimize overshoot, secure rapid settling, and deliver robust steady-state accuracy for DC motor speed control.

$$CLTF(s) = \frac{C_{PI-PDN}(s) \times G_P(s)}{1 + C_{PI-PDN}(s) \times G_P(s)} \quad (27)$$

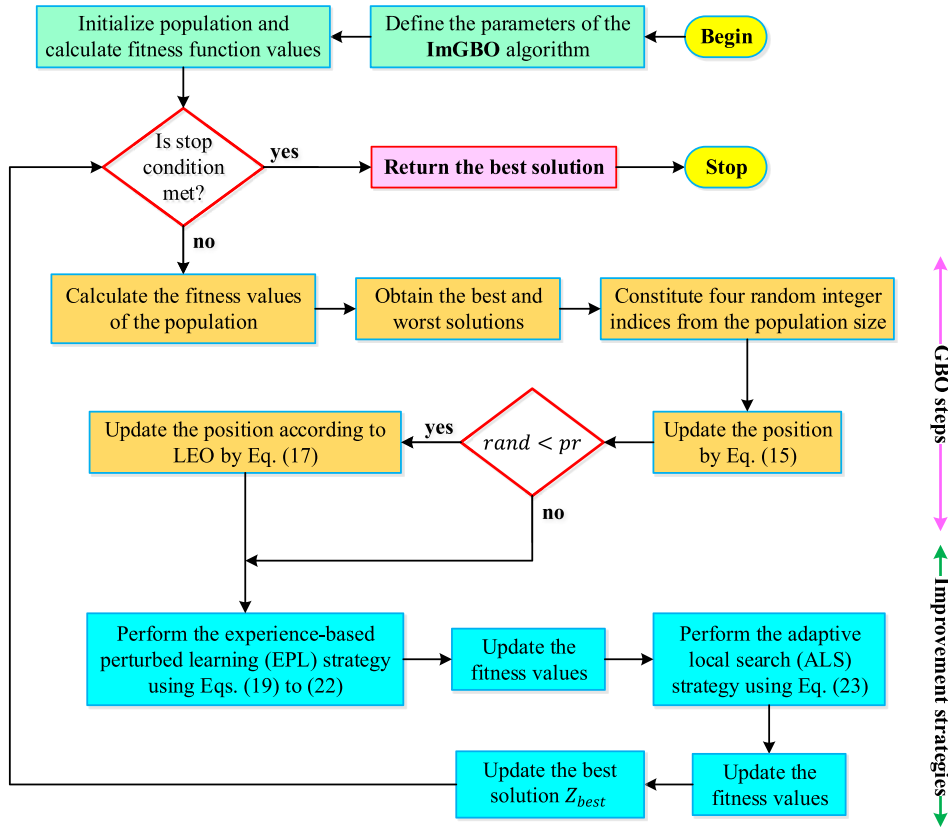


FIGURE 2 | Flowchart of ImGBO algorithm.

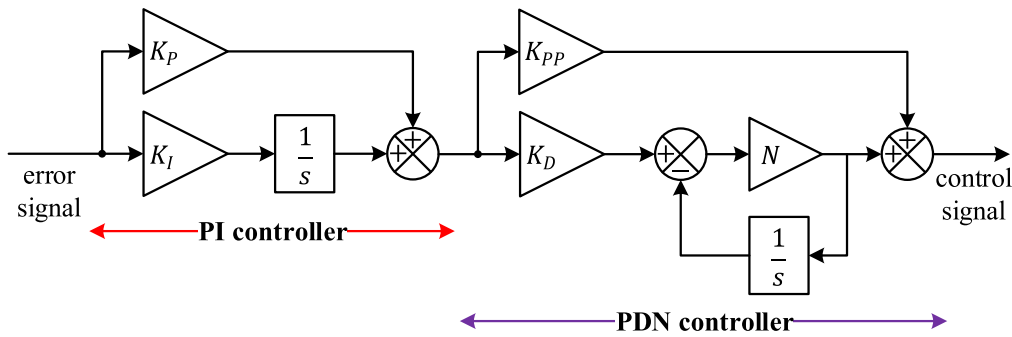


FIGURE 3 | Block diagram of cascaded PI-PDN controller.

#### 4.2 | Constraints of Optimization Problem

Designing the cascaded PI–PDN controller within practical and stable bounds requires formulating an optimization problem that respects preset limits for each control parameter. These limits, shown in Table 1, define allowable ranges for the proportional–integral ( $K_p$ ,  $K_I$ ) and proportional–derivative–filter ( $K_{pp}$ ,  $K_D$ ,  $N$ ) gains. By constraining the controller parameters to these intervals, it is possible to avoid overly aggressive actions that might provoke oscillations or instability, while still affording sufficient flexibility for fine-tuning performance. In this study, the goal is to minimize a designated cost function (the integral of squared error in Equation (30)), with the controller parameters treated as decision variables. Table 1 thus provides crucial

TABLE 1 | Bounds of PI-PDN controller.

Controller parameter	Tuning range
$K_p$	[0.1 – 20]
$K_I$	[0.1 – 20]
$K_{pp}$	[0.1 – 20]
$K_D$	[0.1 – 20]
$N$	[1 – 500]

boundary values that guide the optimization algorithm in exploring only physically plausible or safely implementable controller settings. This approach ensures that, while searching for the ideal gains, the algorithm remains within a space that preserves robustness and operational feasibility of the DC motor speed control system.

### 4.3 | Bode's Ideal Transfer Function-Based Master-Slave Approach and Application of ImGBO Algorithm

In this investigation, a master-slave methodology [42] was employed to enhance the speed regulation performance of a DC motor system. Specifically, an ideal reference model [43–45] was implemented as the master system. The primary objective of the master system is to compel the plant's response to closely track a predefined reference model [46]. Subsequently, the proposed ImGBO was employed as an optimization tool to fine-tune the cascaded PI-PDN controller, serving as the slave system. The ultimate aim is to ensure that the response of the DC motor system effectively adheres to the reference model established by the master system. Equation (28) defines the ideal open loop transfer function, where  $\omega_c$  represents the gain crossover frequency of  $L(s)$ , and  $\alpha$  is a real number within  $0 < \alpha < 2$  [47].

$$L(s) = \left(\frac{\omega_c}{s}\right)^\alpha \quad (28)$$

$\alpha$  determines the slope of the magnitude curve and the phase margin of the system on the Bode plot. The amplitude is a straight line with a constant slope ( $-20\alpha$  dB/dec), and  $-\alpha\pi/2$  rad represents the horizontal line of the phase curve. Consequently, the ideal reference model exhibits robustness against gain variations, maintaining a constant phase margin at  $\pi(1 - \alpha/2)$  rad for varying gain, while only the crossover frequency,  $\omega_c$ , undergoes changes. Equation (29) outlines the description of the ideal closed-loop transfer function model,  $CLTF_{master-slave}(s)$ , with unit feedback.

$$CLTF_{master-slave}(s) = \frac{L(s)}{1 + L(s)} \quad (29)$$

In this particular study, the values of  $\omega_c$  and  $\alpha$  were set to 200 and 1, respectively, for the DC motor system. The ideal reference model functioned as the master system, while the ImGBO-based cascaded PI-PDN controller served as the slave system, ensuring adherence to the ideal response dictated by the ideal reference model.

To address the speed regulation of the DC motor in an effective and practical manner, the problem is conceptualized as a constrained minimization problem, allowing the utilization of optimization algorithms. In outlining the minimization problem, this investigation follows a specific procedure for optimizing the cascaded PI-PDN controller. Initially, the problem is represented as  $X = [x_1, x_2, x_3, x_4, x_5] = [K_P, K_I, K_{PP}, K_D, N]$ . Subsequently, the CF cost function (integral of squared error), given in following equation [48], is employed for effective minimization through the ImGBO.

$$CF = \int_0^{t_f} [e(t)]^2 dt \quad (30)$$

Here,  $t_f$  is simulation time and error signal  $e(t) = \omega_{ref}^*(t) - \omega_{ref}(t)$  represents the error signal, Figure 4 visually depicts the application of the proposed master-slave approach, incorporating the ImGBO-tuned cascaded PI-PDN controller in the DC motor system.

## 5 | Detailed Simulation Results

### 5.1 | Comparison With More Recent Metaheuristic Algorithms

To ensure a fair and comprehensive evaluation of the ImGBO-based PI-PDN controller, its performance has been

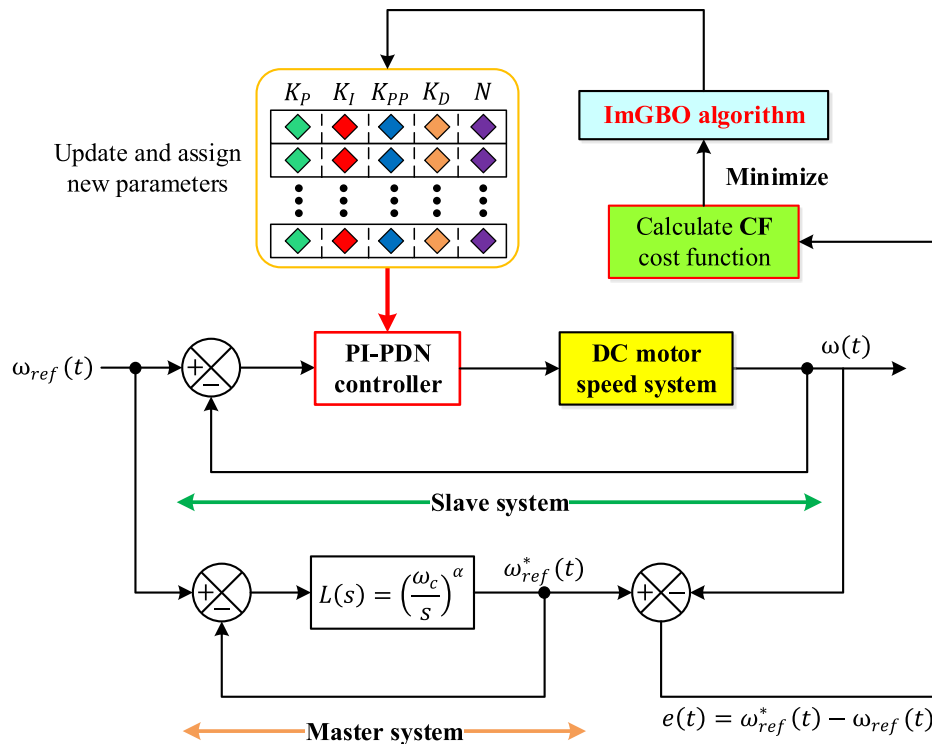


FIGURE 4 | Implementation stage of proposed novel control approach.

compared against several recently developed metaheuristic optimization algorithms. The selection of these algorithms was based on their demonstrated effectiveness in solving complex optimization problems, particularly in the context of control system tuning and dynamic performance enhancement. The GBO [37] was chosen as a baseline for comparison, as it represents the foundational version of the proposed ImGBO. By assessing improvements over its predecessor, we can quantify the advantages introduced by the enhanced mechanisms of EPL and ALS. Additionally, the flood algorithm (FLA) [49] was included in the comparison due to its ability to explore vast search spaces efficiently. FLA has been applied in engineering optimization tasks and has demonstrated promising results in control parameter tuning. However, its effectiveness in fine-tuning control systems remains an open question, making it an important benchmark. Another algorithm considered in this study is the RIME optimizer [50], a physics-inspired metaheuristic that employs a multi-phase search strategy. Given its strong performance in optimization tasks requiring a balance between exploration and exploitation, its inclusion provides insights into how this approach compares against ImGBO. Finally, the artificial hummingbird algorithm (AHA) [51] was selected due to its recent success in dynamic system optimization. AHA mimics the unique foraging behavior of hummingbirds, which enables adaptive search capabilities. Given its relatively recent introduction, evaluating AHA alongside ImGBO offers a direct comparison between a novel bio-inspired approach and the ImGBO technique. By considering these diverse metaheuristic approaches, this study ensures a comprehensive and well-rounded performance assessment. The insights gained from this comparison help establish the significance of ImGBO's improvements in terms of efficiency, accuracy, and robustness in DC motor speed regulation.

## 5.2 | Verification of Statistical Performance of ImGBO

To ensure the reliability and consistency of the ImGBO-based PI-PDN controller, a statistical performance analysis was conducted through 30 independent optimization runs. This approach helps to evaluate how well ImGBO performs across multiple trials, minimizing the influence of randomness in optimization outcomes. Each run consisted of 50 iterations, with a population size of 25, ensuring a robust search for optimal control parameters.

A key metric used for comparison is the integral of squared error (ISE) cost function [48], which directly reflects the control accuracy of the system. Figure 5 presents the ISE values across multiple runs, offering insight into the consistency of the proposed approach. Notably, ImGBO exhibits a lower and more stable error trend compared to other metaheuristic algorithms, indicating its superior ability to fine-tune the controller.

To further support these findings, a boxplot analysis was conducted, as illustrated in Figure 6. This statistical visualization compares the spread and distribution of ISE values for ImGBO, GBO, FLA, RIME, and AHA. The narrower interquartile range and no outliers in the ImGBO results demonstrate its high reliability and minimal performance variance, reinforcing its robustness in controller optimization.

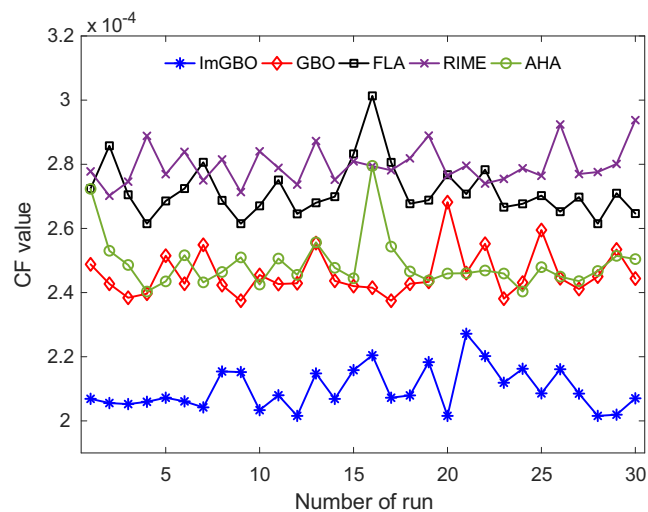


FIGURE 5 | CF cost function values with respect to number of runs.

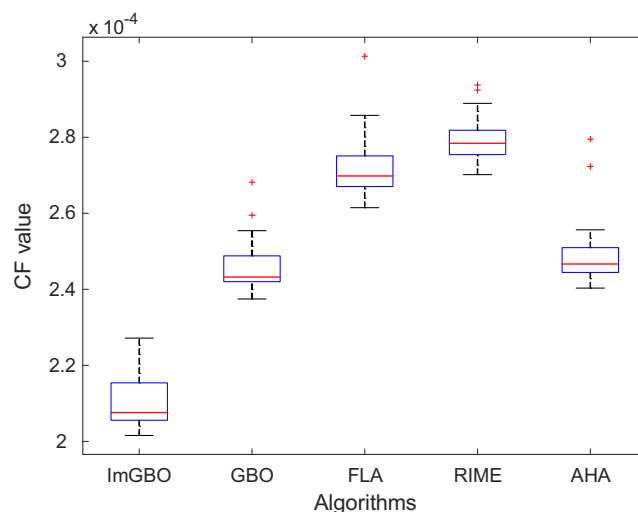
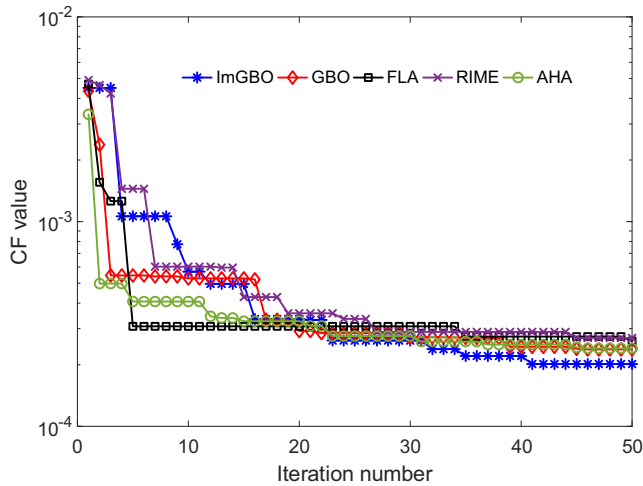


FIGURE 6 | Boxplot analysis results of ImGBO and other algorithms.

Table 2 provides a comprehensive statistical breakdown, including the minimum, maximum, average, standard deviation, and median values for each optimization approach. The results clearly indicate that ImGBO consistently achieves the lowest ISE values across all statistical measures. Additionally, a Wilcoxon rank-sum test [52] was performed to assess the statistical significance of ImGBO's superiority. The extremely low  $p$ -value ( $1.7344E-06$ ) confirms that the improvements offered by ImGBO are not random but are statistically significant compared to other approaches. In summary, the statistical evaluation highlights that ImGBO not only reduces the control error but also maintains stable and repeatable performance, outperforming traditional gradient-based and bio-inspired metaheuristic optimizers. These findings reinforce the suitability of ImGBO for precision-demanding applications, such as DC motor speed regulation, where consistency and efficiency are crucial.

**TABLE 2** | Statistical values and nonparametric results obtained from different algorithms.

Statistical measure	ImGBO	GBO	FLA	RIME	AHA
Minimum	2.0155E-04	2.3746E-04	2.6148E-04	2.7018E-04	2.4032E-04
Maximum	2.2717E-04	2.6819E-04	3.0133E-04	2.9377E-04	2.7952E-04
Average	2.0989E-04	2.4581E-04	2.7169E-04	2.7966E-04	2.4903E-04
Standard deviation	6.5852E-06	7.1425E-06	8.3832E-06	5.8624E-06	8.3071E-06
Median	2.0758E-04	2.4323E-04	2.6983E-04	2.7843E-04	2.4666E-04
<i>p</i> -value (Wilcoxon's test)		1.7344E-06	1.7344E-06	1.7344E-06	1.7344E-06

**FIGURE 7** | Change of CF cost function.

### 5.3 | Convergence Curve of CF Cost Function and Obtained Cascaded PI-PDN Controller Parameters

A crucial component in evaluating the effectiveness and convergence behavior of optimization algorithms is their ability to minimize the selected objective function consistently over iterations. Figure 7 presents the convergence behavior of the ISE cost function (CF) for ImGBO and its comparative algorithms (GBO, FLA, RIME, and AHA) across 50 iterations. At the outset, all algorithms demonstrate a rapid decline in their respective ISE values, which indicates effective initial exploration and quick identification of promising solutions. Particularly the proposed ImGBO distinctly achieves an expedited convergence within roughly the first 10 iterations, surpassing other algorithms by quickly attaining a lower cost function value. After this rapid initial phase, ImGBO continues to incrementally improve its solution, indicating a robust balance between local search refinement and global exploration. In contrast, the other algorithms (GBO, FLA, RIME, and AHA) while initially showing comparable descent, soon exhibit stagnation, settling into higher CF values without notable subsequent improvements. Consequently, Figure 7 underscores ImGBO's superior capability to consistently and effectively minimize the cost function, reflecting its enhanced optimization mechanisms. These mechanisms ensure that the cascaded PI-PDN controller parameters tuned by ImGBO are not only rapidly identified but also finely adjusted for optimal and stable performance.

**TABLE 3** | The obtained controller parameters via ImGBO, GBO, FLA, RIME, and AHA algorithms.

Controller parameter	ImGBO	GBO	FLA	RIME	AHA
$K_P$	4.0143	2.5612	4.0514	7.5973	3.5372
$K_I$	14.1642	11.6480	8.2732	19.0290	0.7604
$K_{PP}$	0.9032	1.4577	1.4919	2.4694	10.6526
$K_D$	3.2263	4.7603	3.0918	1.6227	3.5340
$N$	495.4773	477.4096	496.0636	440.2394	486.9943

Further supporting these insights, Table 3 lists the optimized cascaded PI-PDN controller parameters obtained through ImGBO alongside those achieved by the benchmarked algorithms. These values reflect a well-tuned controller capable of handling disturbances efficiently, achieving rapid transient response, and maintaining robust steady-state stability. In comparison, while the other algorithms produce parameter sets that sometimes show individual gains higher or lower, none demonstrate the cohesive optimization evident in ImGBO's result. For instance, RIME shows an overly aggressive proportional gain coupled with a comparatively low derivative gain, potentially leading to oscillatory or less stable system behavior. Conversely, AHA's substantially higher derivative gain alongside a lower integral gain indicates a susceptibility to noise amplification and inadequate steady-state error compensation. The outcomes encapsulated in Figure 7 and Table 3 reinforce the superiority of ImGBO in effectively navigating the optimization landscape. This superior performance stems from its adaptive local search mechanism and experience-based perturbed learning strategy, providing a robust optimization method that balances exploration and exploitation proficiently. Consequently, ImGBO emerges as a highly competent and recommended approach for the cascaded PI-PDN controller tuning in DC motor speed regulation applications.

### 5.4 | Time Response Analysis

This section meticulously examines the time-domain performance of the cascaded PI-PDN controller tuned by the ImGBO algorithm, systematically comparing its responses with those of GBO, FLA, RIME, and AHA algorithms. Initially, Table 4 provides the derived closed-loop transfer functions for each considered algorithm. These transfer functions clearly indicate the differences in system dynamics resulting from distinct tuning methods. Each transfer function encapsulates the controller's unique influence on the system's speed regulation characteristics.

**TABLE 4** | The obtained closed-loop transfer functions for ImGBO, GBO, FLA, RIME, and AHA algorithms.

Algorithm	CLTF(s) (closed-loop transfer function)
ImGBO	$\frac{96.31s^2+366.8s+95.08}{0.00108s^4+0.5412s^3+99.33s^2+367.6s+95.08}$
GBO	$\frac{87.37s^2+424.1s+121.6}{0.00108s^4+0.5217s^3+90.28s^2+424.8s+121.6}$
FLA	$\frac{93.3s^2+235.5s+91.84}{0.00108s^4+0.5418s^3+96.32s^2+236.3s+91.84}$
RIME	$\frac{81.69s^2+328.5s+310.3}{0.00108s^4+0.4816s^3+84.38s^2+329.2s+310.3}$
AHA	$\frac{91.88s^2+295s+59.17}{0.00108s^4+0.5321s^3+94.85s^2+295.8s+59.17}$

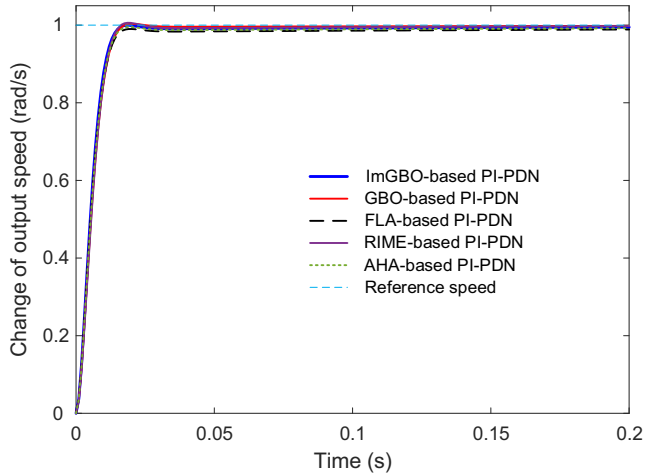


**FIGURE 8** | Step response for change of output speed.

Figure 8 illustrates the complete step response of the output speed for all controller approaches. It clearly highlights the rapid response and lack of overshoot exhibited by the ImGBO-based PI-PDN controller compared to the other methods. The ImGBO algorithm demonstrates superior dynamic stability and quicker settling to the desired speed. To provide clearer insights, Figure 9 offers an enlarged view of Figure 8's response curves. This magnified visualization distinctly emphasizes the smooth transient response of the ImGBO-based controller, further affirming its superior performance with no discernible overshoot and rapid stabilization.

The steady-state response analysis depicted in Figure 10 further confirms ImGBO's excellent tracking capability, maintaining stable and precise output speeds. In contrast, other algorithms show slight oscillations and reduced precision in their steady-state behavior.

Table 5 complements these visual assessments by summarizing key performance metrics, including rise time, settling time, overshoot percentage, and steady-state error percentage. The ImGBO-based controller notably outperforms others, with the shortest rise time (0.0089 s), quickest settling time (0.0140 s), no overshoot, and a minimal steady-state error (0.0017%). Contrarily, the other controllers present less favorable metrics, especially RIME with the highest overshoot (0.6210%) and considerable steady-state error (0.1118%).

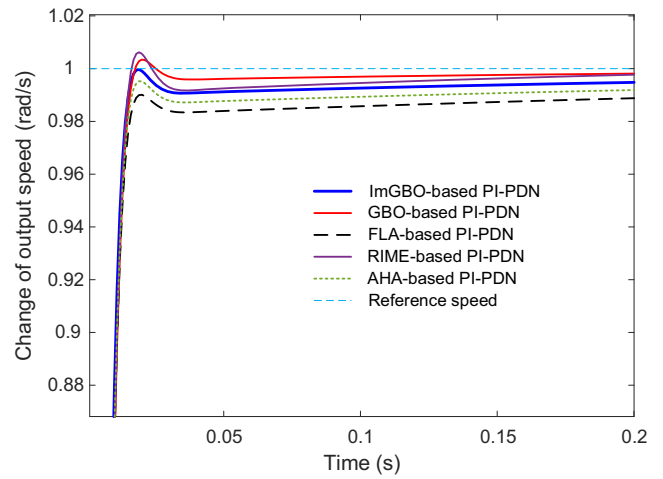


**FIGURE 9** | Enlarged version of Figure 8.

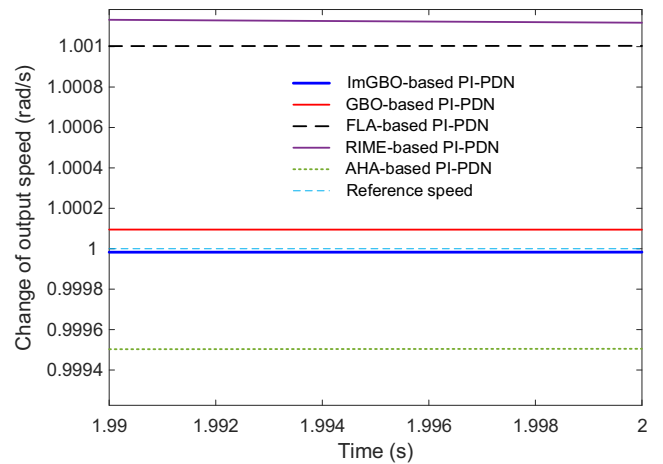


**FIGURE 10** | Steady-state response analysis of ImGBO, GBO, FLA, RIME, and AHA based PI-PDN controllers.

**TABLE 5** | Time response metrics for ImGBO, GBO, FLA, RIME, and AHA based PI-PDN controllers.

Control approach	Rise time (s)	Settling time (s)	Overshoot (%)	Steady-state error (%)
ImGBO-based PI-PDN	<b>0.0089</b>	<b>0.0140</b>	<b>0</b>	<b>0.0017</b>
GBO-based PI-PDN	0.0093	0.0147	0.3413	0.0094
FLA-based PI-PDN	0.0093	0.0157	0.1004	0.1004
RIME-based PI-PDN	0.0091	0.0142	0.6210	0.1118
AHA-based PI-PDN	0.0092	0.0149	<b>0</b>	0.0495

## 5.5 | Controller Efforts

The assessment of controller effort is crucial to understand the practical implications and efficiency of various tuning methods in control systems [53]. In this section, we provide a comprehensive evaluation of the controller efforts for the ImGBO-based cascaded PI-PDN controller alongside its comparative algorithms. Table 6 quantitatively summarizes these efforts by presenting two critical metrics: the overall magnitude of the control signal and the energy consumed by each controller method. The

**TABLE 6** | Controller efforts for ImGBO, GBO, FLA, RIME, and AHA based PI-PDN approaches.

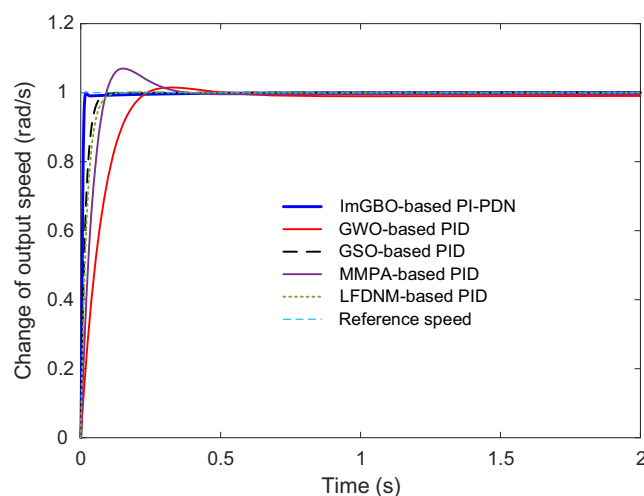
Control approach	$U_{max}$	Energy
ImGBO-based PI-PDN	6.4207E+03	4.1504E+04
GBO-based PI-PDN	5.8243E+03	3.5514E+04
FLA-based PI-PDN	6.2198E+03	3.8802E+04
RIME-based PI-PDN	5.4461E+03	3.3593E+04
AHA-based PI-PDN	6.1253E+03	3.8380E+04

ImGBO-based PI-PDN controller records a control signal magnitude of  $6.4207 \times 10^3$  and an energy expenditure of  $4.1504 \times 10^4$ . While these values represent slightly higher demands compared to those of some alternative controllers, such as the RIME-based method, which exhibits the lowest values (control signal:  $5.4461 \times 10^3$ , energy:  $3.3593 \times 10^4$ ), the increased effort of the ImGBO-based controller is directly linked to its superior performance and precision in controlling the DC motor speed. The data from Table 6 reveal a trade-off commonly encountered in controller design: enhanced performance typically necessitates greater control effort. However, this additional effort required by the ImGBO-based PI-PDN controller is justified by the significant improvement in key dynamic performance indicators such as rapid rise time, minimized settling time, absence of overshoot, and extremely low steady-state errors. In comparison, although algorithms like GBO, FLA, and AHA show slightly reduced control signal magnitudes and energy expenditures, their inferior control performance metrics, particularly in terms of overshoot and steady-state accuracy, highlight that their efficiency comes at the cost of reduced control quality.

## 5.6 | Comparison With Recently Documented PID Controllers

This section expands the comparative analysis by assessing the performance of the proposed ImGBO-based cascaded PI-PDN controller against recently documented PID controllers optimized by various contemporary metaheuristic algorithms. Specifically, this analysis includes comparisons with controllers tuned by the grey wolf optimizer (GWO)-based PID [54], gazelle simplex optimizer (GSO)-based PID [55], improved model of marine predator algorithm (MMPA)-based PID [56], and hybrid Lévy flight distribution and Nelder–Mead algorithm (LFDNM)-based PID [57] controllers. Figure 11 visually demonstrates the step response performance comparison of the proposed ImGBO-based approach relative to the PID controllers tuned using the aforementioned recent algorithms. The ImGBO-tuned controller clearly exhibits a distinctly superior performance, characterized by an exceptionally rapid response with zero overshoot, showcasing remarkable dynamic stability.

Table 7 provides a detailed numerical analysis, further clarifying the performance disparities among the approaches. The ImGBO-based PI-PDN controller achieves the shortest rise time (0.0089 s), quickest settling time (0.0140 s), and an impressive near-zero steady-state error (0.0017%). Notably, it completely avoids overshoot. In comparison, the GWO-based PID controller displays a notably higher rise time (0.1388 s), prolonged settling

**FIGURE 11** | Speed comparison of the proposed approach with respect to recently documented PID controllers.**TABLE 7** | Numerical comparison of time response metrics with respect to recently documented PID controllers.

Control approach	Rise time (s)	Settling time (s)	Overshoot (%)	Steady-state error (%)
ImGBO-based PI-PDN	<b>0.0089</b>	<b>0.0140</b>	<b>0</b>	<b>0.0017</b>
GWO-based PID	0.1388	0.2052	1.5068	0.9505
GSO-based PID	0.0365	0.0650	0	0.0080
MMPA-based PID	0.0635	0.2793	7.0060	0.4358
LFDNM-based PID	0.0462	0.0813	0.0676	0.0051

time (0.2052 s), significant overshoot (1.5068%), and substantial steady-state error (0.9505%). Similarly, the MMPA-tuned PID demonstrates even more pronounced deficiencies, with an extensive overshoot (7.0060%) and a high steady-state error (0.4358%). While GSO and LFDNM-tuned PID controllers perform relatively better, their metrics still significantly lag behind those achieved by the ImGBO-based method.

## 5.7 | Comparison With Recently Documented FOPID Controllers

In this section, the performance of the proposed ImGBO-based cascaded PI-PDN controller is compared against several recently developed fractional-order PID (FOPID) controllers. These controllers are optimized by advanced metaheuristic techniques, including the improved artificial rabbits optimizer (IARO)-based FOPID [58], hybrid stochastic fractal search (HSFS)-based FOPID [59], manta ray foraging optimizer (MRFO)-based FOPID [35], and chaotic atom search optimization (ChASO)-based FOPID [36] controllers. Figure 12 visually presents the comparative step responses for these advanced control methods. The figure clearly highlights the ImGBO-based cascaded PI-PDN controller's superior performance, characterized by significantly faster rise time, shorter settling time, and complete elimination of overshoot. These attributes underscore its exceptional capability for rapid and stable tracking of desired speed trajectories.

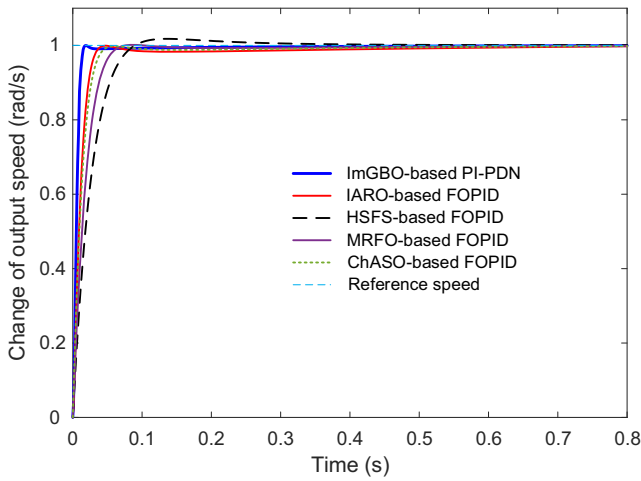


**FIGURE 12** | Speed comparison of the proposed approach with respect to recently documented FOPID controllers.

**TABLE 8** | Numerical comparison of time response metrics with respect to recently documented FOPID controllers.

Control approach	Rise time (s)	Settling time (s)	Overshoot (%)	Steady-state error (%)
ImGBO-based PI-PDN	<b>0.0089</b>	<b>0.0140</b>	<b>0</b>	<b>0.0017</b>
IARO-based FOPID	0.0205	0.0330	0.4964	0.4964
HSFS-based FOPID	0.0505	0.0766	1.7659	0.0436
MRFO-based FOPID	0.0355	0.0562	0.1520	0.0324
ChASO-based FOPID	0.0253	0.0406	0.0610	0.0591

Complementing this visual analysis, Table 8 provides quantitative comparisons by explicitly detailing the rise time, settling time, overshoot percentage, and steady-state error percentage for each controller method. Remarkably, the ImGBO-tuned controller records the shortest rise time (0.0089 s) and fastest settling time (0.0140 s), coupled with zero overshoot and minimal steady-state error (0.0017%). In contrast, the IARO-based FOPID controller exhibits a relatively slower rise time (0.0205 s) and settling time (0.0330 s), along with notable overshoot (0.4964%) and significantly higher steady-state error (0.4964%). Similarly, the HSFS-based FOPID shows considerable overshoot (1.7659%) and steady-state error (0.0436%), while MRFO and ChASO-based FOPIDs perform moderately better but still lag substantially behind the proposed ImGBO-based controller. This comprehensive comparative analysis clearly demonstrates the robust and precise performance advantages offered by the ImGBO-based cascaded PI-PDN controller. Its superior time-domain characteristics strongly affirm its suitability as an advanced, practical, and reliable controller for high-performance DC motor speed regulation.

### 5.8 | Verification of Master/Slave Model-Driven Cascaded PI-PDN Controller Tuned With the ImGBO

In this section, we validate the effectiveness and reliability of the proposed master–slave architecture integrated with the

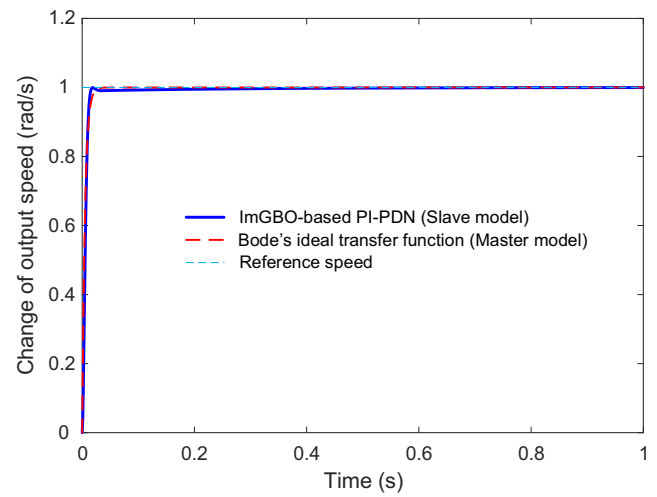


**FIGURE 13** | Time response comparison of slave and master models.

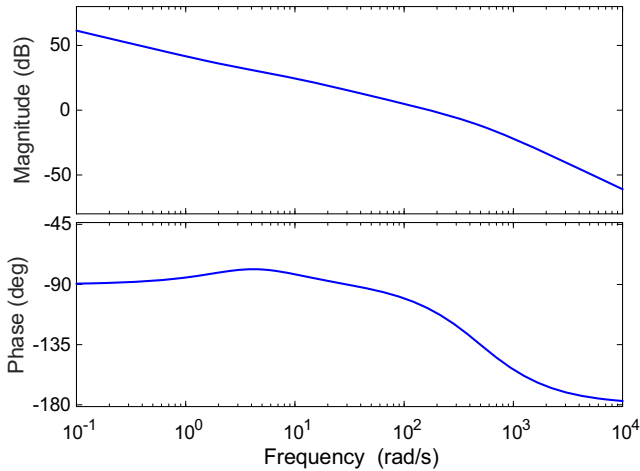
ImGBO-tuned cascaded PI-PDN controller. The verification focuses on assessing the alignment between the designed slave system's response and the prescribed master reference model. Figure 13 explicitly demonstrates the comparative time-domain responses of both the master reference model and the slave system employing the ImGBO-based cascaded PI-PDN controller. From Figure 13, it is clearly observable that the response of the slave system closely mirrors the response provided by the master model. This congruence confirms the appropriateness and efficacy of the chosen design parameters, particularly the selected crossover frequency ( $\omega_c = 200$ ) and the slope factor ( $\alpha = 1$ ), ensuring the slave system accurately follows the predefined ideal performance criteria established by the master system. The highly precise matching of these two models underscores the robustness of the proposed controller design strategy. The ImGBO optimization effectively identifies optimal parameters for the cascaded PI-PDN controller, allowing the slave system to achieve near-perfect adherence to the master system's reference trajectory. This alignment ensures not only rapid and stable responses but also robust performance under various operational conditions.

### 5.9 | Stability Analysis of Proposed ImGBO-Based PI-PDN Controller

In this section, we present a comprehensive stability analysis to examine the robustness and reliability of the proposed ImGBO-based cascaded PI-PDN controller. The stability of a control system is a fundamental requirement, essential for ensuring safe and predictable operation under various operating conditions. Table 9 outlines the numerical results from the pole analysis, detailing the pole locations, damping ratios, and natural frequencies. The data clearly demonstrate that all system poles are located in the left half-plane, confirming the inherent stability of the closed-loop system. Specifically, the real-valued poles at  $-0.2798$  and  $-3.4923$  indicate stable, non-oscillatory modes. Furthermore, the complex conjugate poles at  $-248.68 \pm j168.11$  exhibit a high damping ratio of 0.8285, signifying rapid attenuation of oscillations and reinforcing the robust dynamic response of the system.

**TABLE 9** | Numerical values obtained from stability analysis.

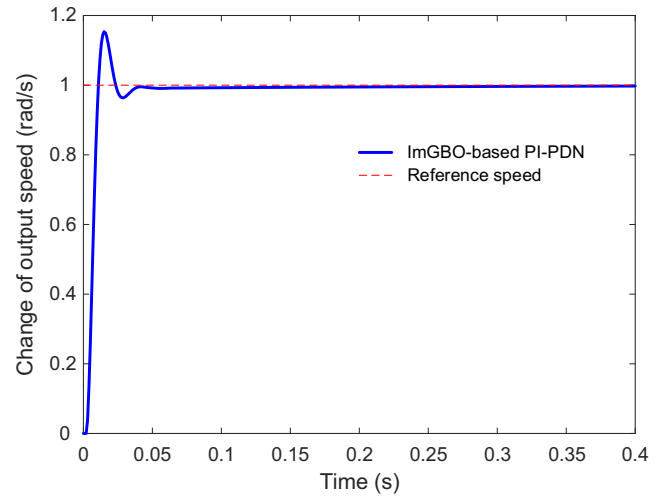
Pole	Damping	Frequency (rad/s)
-0.2798	1	0.2798
-3.4923	1	3.4923
-248.68 + j168.11	0.8285	300.1660
-248.68 - j168.11	0.8285	300.1660

**FIGURE 14** | Bode plot of open-loop system with proposed ImGBO-based PI-PDN controller.

To further support these findings, Figure 14 presents the Bode plot analysis, illustrating the frequency response characteristics of the open-loop system when equipped with the proposed ImGBO-based cascaded PI-PDN controller. The Bode plot analysis reveals critical stability margins and bandwidth: the gain margin is infinite, clearly indicating that the system is highly tolerant to gain changes without losing stability, and the phase margin is notably high at  $71.6640^\circ$ , highlighting substantial robustness against phase perturbations. Additionally, the calculated bandwidth of 246.2469 rad/s signifies the controller's capability to handle rapid changes in the input command efficiently and accurately. Collectively, these stability metrics confirm that the ImGBO-tuned cascaded PI-PDN controller not only achieves excellent dynamic performance but also ensures robust stability across a wide range of operational scenarios. This analysis emphasizes the practical applicability and reliability of the proposed control strategy for DC motor speed regulation tasks.

### 5.10 | Performance Evaluation Under Time Delay and Actuator Saturation

To assess the robustness of the proposed ImGBO-based PI-PDN controller under practical constraints, an additional simulation was carried out incorporating a control input saturation of  $\pm 200$  and a time delay of 0.002 s. These conditions emulate common nonlinearities found in real-time systems, such as actuator limitations and communication delays. As illustrated in Figure 15, the controller maintains excellent tracking performance despite the introduced challenges. The system exhibits only minor overshoot and quickly stabilizes, closely following the reference speed. This

**FIGURE 15** | Output speed response under time delay ( $t_d = 0.002$  s) and saturation limit ( $\pm 2000$ ).

result demonstrates the robustness of the proposed control strategy and highlights its strong potential for real-time applications involving nonlinear components and delay-sensitive systems.

## 6 | Conclusion

In this research, a cascaded PI-PDN controller tuned through the proposed ImGBO was developed and thoroughly tested for the DC motor speed regulation task. The principal novelty and contribution of this study stem from the introduction of experience-based perturbed learning and adaptive local search strategies within the traditional GBO framework. These enhancements significantly improved the optimization efficiency, leading to substantial improvements in the performance metrics of the cascaded PI-PDN controller. Simulation comparisons revealed the superiority of the ImGBO-tuned controller over traditional GBO, recent metaheuristic methods, and advanced PID and FOPID controllers. The ImGBO-based controller achieved remarkable transient dynamics, evidenced by a rise time of 0.0089 s, settling time of 0.0140 s, zero overshoot, and steady-state error of only 0.0017%. Additionally, rigorous stability analyses confirmed robust system performance, achieving a notably high phase margin ( $71.6640^\circ$ ) and an infinite gain margin, reinforcing the reliability and robustness of the proposed method. Beyond the transient and steady-state advantages, the proposed controller also performed well under energy considerations. Although the controller effort was slightly higher than that of certain alternatives, the trade-off was justified by the significant improvements in precision and response time.

Future research can build upon the findings of this study in several meaningful directions. A primary avenue involves the experimental validation of the proposed ImGBO-based cascaded PI-PDN controller on a physical DC motor setup, which would offer critical insights into its real-world performance and the practical challenges associated with implementation. Additionally, the adaptability of the ImGBO framework could be explored in more complex or nonlinear systems, such as robotic manipulators, multi-motor coordination platforms, and renewable energy

conversion systems, where dynamic conditions and uncertainties pose greater control challenges. Another promising direction lies in the integration of real-time adaptation mechanisms or hybrid intelligent strategies, which could further strengthen the controller's robustness in dynamically changing environments. Moreover, the application of multi-objective optimization techniques would allow the controller to address multiple performance criteria simultaneously, such as minimizing energy consumption, suppressing control-induced noise, and achieving smoother actuation, all of which are crucial in industrial and embedded applications. Collectively, these directions not only offer opportunities to enhance the practicality and versatility of the proposed control strategy but also underscore its potential to serve as a reliable and high-performing solution in diverse real-world control scenarios.

### Author Contributions

**Davut Izci and Serdar Ekinci:** conceptualization, methodology, software, visualization, investigation, writing – original draft preparation.

**Other Authors:** validation, supervision, resources, writing – review and editing.

### Acknowledgments

This work was supported by Princess Nourah Bint Abdulrahman University Researchers Supporting Project number (PNURSP2025R594), Princess Nourah Bint Abdulrahman University, Riyadh, Saudi Arabia. The authors gratefully acknowledge financial support from the European Union under the REFRESH—Research Excellence For REgion Sustainability and High-tech Industries project number CZ.10.03.01/00/22\_/0000048 via the Operational Programme Just Transition. This research was co-funded by the European Union under the project ROBOPROX (reg. no. CZ.02.01.01/00/22\_008/0004590), and by the internal grant project Processing and advanced analysis of biomedical data IX, project no. SP2024/007.

### Ethics Statement

This article does not contain any studies with human participants or animals performed by any of the authors.

### Consent

Informed consent was obtained from all individual participants included in the study.

### Conflicts of Interest

The authors declare no conflicts of interest.

### Data Availability Statement

The data that support the findings of this study are available from the corresponding author upon reasonable request.

### References

1. R. Akbari-Hasanjani, S. Javadi, and R. Sabbaghi-Nadooshan, "DC Motor Speed Control by Self-Tuning Fuzzy PID Algorithm," *Transactions of the Institute of Measurement and Control* 37 (2015): 164–176, <https://doi.org/10.1177/0142331214535619>.
2. S.-C. Chen and C.-Y. Kuo, "Design and Implementation of Double-Integral Sliding-Mode Controller for Brushless Direct Current Motor Speed Control," *Advances in Mechanical Engineering* 9 (2017): 168781401773772, <https://doi.org/10.1177/1687814017737724>.

3. S. Ekinci, D. Izci, M. H. Almomani, et al., "Advanced Control Parameter Optimization in DC Motors and Liquid Level Systems," *Scientific Reports* 15 (2025): 1394, <https://doi.org/10.1038/s41598-025-85273-y>.
4. D. Puangdownreong, "Optimal PID Controller Design for DC Motor Speed Control System With Tracking and Regulating Constrained Optimization via Cuckoo Search," *Journal of Electrical Engineering and Technology* 13 (2018): 460–467, <https://doi.org/10.5370/JEET.2018.13.1.460>.
5. Y. Guo and M. E. A. Mohamed, "Speed Control of Direct Current Motor Using ANFIS Based Hybrid P-I-D Configuration Controller," *IEEE Access* 8 (2020): 125638–125647, <https://doi.org/10.1109/ACCESS.2020.3007615>.
6. D. Izci, S. Ekinci, H. L. Zeynelgil, and J. Hedley, "Fractional Order PID Design Based on Novel Improved Slime Mould Algorithm," *Electric Power Components & Systems* 49 (2021): 901–918, <https://doi.org/10.1080/15325008.2022.2049650>.
7. M. Jabari, S. Ekinci, D. Izci, M. Bajaj, and I. Zaitsev, "Efficient DC Motor Speed Control Using a Novel Multi-Stage FOPD(1 + PI) Controller Optimized by the Pelican Optimization Algorithm," *Scientific Reports* 14 (2024): 22442, <https://doi.org/10.1038/s41598-024-73409-5>.
8. E. Eker, M. Kayri, S. Ekinci, and D. Izci, "A New Fusion of ASO With SA Algorithm and Its Applications to MLP Training and DC Motor Speed Control," *Arabian Journal for Science and Engineering* 46 (2021): 3889–3911, <https://doi.org/10.1007/s13369-020-05228-5>.
9. R. Zare, H. Mohajery, and P. Shayeghi, "Optimal FOTID Controller Design for Regulation of DC Motor Speed," *International Journal on Technical and Physical Problems of Engineering* 14 (2022): 57–63.
10. G. Lloyds Raja and A. Ali, "New PI-PD Controller Design Strategy for Industrial Unstable and Integrating Processes With Dead Time and Inverse Response," *Journal of Control, Automation and Electrical Systems* 32 (2021): 266–280, <https://doi.org/10.1007/s40313-020-00679-5>.
11. G. L. Raja, "Enhanced Design of a PI-PD Based Smith Predictor for Industrial Plants," *IFAC-PapersOnLine* 54 (2021): 79–84, <https://doi.org/10.1016/j.ifacol.2021.12.014>.
12. D. Das, S. Chakraborty, and G. L. Raja, "Enhanced Dual-DOF PI-PD Control of Integrating-Type Chemical Processes," *International Journal of Chemical Reactor Engineering* 21 (2023): 907–920, <https://doi.org/10.1515/ijcre-2022-0156>.
13. A. Sagar, R. Radhakrishnan, and G. L. Raja, "Cascade Plus Feed Forward Control Strategy for Enhanced Regulation in Maglev System," *IFAC-PapersOnLine* 57 (2024): 355–360, <https://doi.org/10.1016/j.ifacol.2024.05.061>.
14. P. Singha, D. Das, S. Chakraborty, and G. Lloyds Raja, "Experimentally Validated Predictive PI-PD Control Strategy for Delay-Dominant Chemical Processes," *Chemical Engineering Science* 295 (2024): 120197, <https://doi.org/10.1016/j.ces.2024.120197>.
15. D. Sridhar, G. L. Kumar, S. Raja, and S. Chakraborty, "Relocated Internal Model Based Cascade Control Strategy for Stable and Unstable Systems With Delay," *International Journal of Systems Science* 55 (2024): 499–516, <https://doi.org/10.1080/00207721.2023.2281881>.
16. J. A. Prakosa, A. Gusrialdi, E. Kurniawan, A. D. Stotckaia, H. Adinanta, and Suryadi, "Experimentally Robustness Improvement of DC Motor Speed Control Optimization by H-Infinity of Mixed-Sensitivity Synthesis," *International Journal of Dynamics and Control* 10 (2022): 1968–1980, <https://doi.org/10.1007/s40435-022-00956-y>.
17. S. Subramani, K. K. Vijayarangan, and M. Chenniappan, "Improved African Buffalo Optimization-Based Takagi–Sugeno–Kang Fuzzy PI Controller for Speed Control in BLDC Motor," *Electric Power Components & Systems* 51 (2023): 1948–1962, <https://doi.org/10.1080/15325008.2023.2210570>.
18. P. Aryan, G. L. Raja, and R. Vilanova, "Equilibrium Optimiser Tuned Frequency-Shifted Internal Model Control Proportional-Derivative

- Decoupled Dual-Loop Design for Industrial Plants Followed by Experimental Validation,” *International Journal of Systems Science* 55 (2024): 2874–2896, <https://doi.org/10.1080/00207721.2024.2363544>.
19. Z. A. Ansari and G. L. Raja, “Flow Direction Optimizer Tuned Robust FOPID-(1 + TD) Cascade Controller for Oscillation Mitigation in Multi-Area Renewable Integrated Hybrid Power System With Hybrid Electrical Energy Storage,” *Journal of Energy Storage* 83 (2024): 110616, <https://doi.org/10.1016/j.est.2024.110616>.
20. P. Aryan, G. Lloyds Raja, R. Vilanova, and M. Meneses, “Repositioned Internal Model Control Strategy on Time-Delayed Industrial Processes With Inverse Behavior Using Equilibrium Optimizer,” *IEEE Access* 11 (2023): 54556–54568, <https://doi.org/10.1109/ACCESS.2023.3281691>.
21. P. Aryan and G. L. Raja, “A Novel Equilibrium Optimized Double-Loop Control Scheme for Unstable and Integrating Chemical Processes Involving Dead Time,” *International Journal of Chemical Reactor Engineering* 20 (2022): 1341–1360, <https://doi.org/10.1515/ijcre-2022-0007>.
22. A. Anand, P. Aryan, N. Kumari, and G. L. Raja, “Type-2 Fuzzy-Based Branched Controller Tuned Using Arithmetic Optimizer for Load Frequency Control,” *Energy Sources, Part A: Recovery, Utilization, and Environmental Effects* 44 (2022): 4575–4596, <https://doi.org/10.1080/15567036.2022.2078444>.
23. S. L. Ayinla, T. I. Amosa, O. Ibrahim, et al., “Optimal Control of DC Motor Using Leader-Based Harris Hawks Optimization Algorithm,” *Franklin Open* 6 (2024): 100058, <https://doi.org/10.1016/j.fraope.2023.100058>.
24. A. F. Güven, O. Ö. Mengi, M. A. Elseify, and S. Kamel, “Comprehensive Optimization of PID Controller Parameters for DC Motor Speed Management Using a Modified Jellyfish Search Algorithm,” *Optimal Control Applications and Methods* 46 (2025): 320–342, <https://doi.org/10.1002/oca.3218>.
25. E. Çelik, G. Bal, N. Öztürk, et al., “Improving Speed Control Characteristics of PMDC Motor Drives Using Nonlinear PI Control,” *Neural Computing & Applications* 36 (2024): 9113–9124, <https://doi.org/10.1007/s00521-024-09568-3>.
26. M. Peram, S. Mishra, M. Vemulapaty, B. Verma, and P. K. Padhy, “Optimal PI-PD and I-PD Controller Design Using Cuckoo Search Algorithm,” in *2018 5th International Conference on Signal Processing and Integrated Networks (SPIN)* (IEEE, 2018), 643–646, <https://doi.org/10.1109/SPIN.2018.8474214>.
27. C. Copot, C. I. Muresan, and R. DeKeyser, “Speed and Position Control of a DC Motor Using Fractional Order PI-PD Control,” in *3rd International Conference on Fractional Signals and Systems (FSS-2013)* (IEEE, 2013).
28. S. Singh and A. Kosti, “Comparative Study of Integer Order PI-PD Controller and Fractional Order PI-PD Controller of a DC Motor for Speed and Position Control,” *International Journal of Electrical and Electronic Engineering & Telecommunications* 4 (2015): 22–26.
29. B. Çavdar, E. Sahin, and F. Nuroglu, “Doğru Akım Motoru Hız Kontrolü İçin SAA Tabanlı Kesir Dereceli PI-PD Eklemeli Denetleyici Tasarımı,” *Politeknik Dergisi* 27 (2024): 283–296, <https://doi.org/10.2339/politeknik.1139517>.
30. V. K. Singh, S. Sharma, and P. K. Padhy, “Controlling of AVR Voltage and Speed of DC Motor Using Modified PI-PD Controller,” in *2018 2nd IEEE International Conference on Power Electronics, Intelligent Control and Energy Systems (ICPEICES)* (IEEE, 2018), 858–863, <https://doi.org/10.1109/ICPEICES.2018.8897302>.
31. F. Alyoussef, I. Kaya, and A. Akrad, “Robust PI-PD Controller Design: Industrial Simulation Case Studies and a Real-Time Application,” *Electronics (Basel)* 13 (2024): 3362, <https://doi.org/10.3390/electronics13173362>.
32. N. Naajihah Ab Rahman and N. Mat Yahya, “System Identification for a Mathematical Model of DC Motor System,” in *2022 IEEE International Conference on Automatic Control and Intelligent Systems (I2CACIS)* (IEEE, 2022), 30–35, <https://doi.org/10.1109/I2CACIS4679.2022.9815461>.
33. N. N. A. Rahman and N. M. Yahya, “A Mathematical Model of a Brushed DC Motor System,” *Data Analytics and Applied Mathematics (DAAM)* 2 (2021): 60–68, <https://doi.org/10.15282/daam.v2i2.6830>.
34. J.-H. Jang and S.-H. Kim, “A PI-PD Controller Design for the Position Control of a Motor,” *Transactions of the Korean Institute of Power Electronics* 22 (2017): 60–66, <https://doi.org/10.6113/TKPE.2017.22.1.60>.
35. S. Ekinci, D. Izci, and B. Hekimoğlu, “Optimal FOPID Speed Control of DC Motor via Opposition-Based Hybrid Manta Ray Foraging Optimization and Simulated Annealing Algorithm,” *Arabian Journal for Science and Engineering* 46 (2021): 1395–1409, <https://doi.org/10.1007/s13369-020-05050-z>.
36. B. Hekimoglu, “Optimal Tuning of Fractional Order PID Controller for DC Motor Speed Control via Chaotic Atom Search Optimization Algorithm,” *IEEE Access* 7 (2019): 38100–38114, <https://doi.org/10.1109/ACCESS.2019.2905961>.
37. I. Ahmadianfar, O. Bozorg-Haddad, and X. Chu, “Gradient-Based Optimizer: A New Metaheuristic Optimization Algorithm,” *Information Sciences (New York)* 540 (2020): 131–159, <https://doi.org/10.1016/j.ins.2020.06.037>.
38. R. M. Rizk-Allah, S. Ekinci, and D. Izci, “An Improved Artificial Rabbits Optimization for Accurate and Efficient Infinite Impulse Response System Identification,” *Decision Analytics Journal* 9 (2023): 100355, <https://doi.org/10.1016/j.dajour.2023.100355>.
39. S. Ekinci, D. Izci, O. Can, M. Bajaj, and V. Blazek, “Frequency Regulation of PV-Reheat Thermal Power System via a Novel Hybrid Educational Competition Optimizer With Pattern Search and Cascaded PDN-PI Controller,” *Results in Engineering* 24 (2024): 102958, <https://doi.org/10.1016/j.rineng.2024.102958>.
40. S. Ekinci, D. Izci, R. Ghandour, M. Salman, and C. Turkeri, “Aquila Optimizer-Based Filtered PID Controller Design for A Spark Ignition Engine Speed Control,” in *2024 8th International Symposium on Innovative Approaches in Smart Technologies (ISAS)* (IEEE, 2024), 1–5, <https://doi.org/10.1109/ISAS64331.2024.10845268>.
41. S. K. Ojha and C. O. Maddela, “Load Frequency Control of a Two-Area Power System With Renewable Energy Sources Using Brown Bear Optimization Technique,” *Electrical Engineering* 106, no. 3 (2023): 3589–3613, <https://doi.org/10.1007/s00202-023-02143-4>.
42. D. Izci, S. Ekinci, S. Mirjalili, and L. Abugaligh, “An Intelligent Tuning Scheme With a Master/Slave Approach for Efficient Control of the Automatic Voltage Regulator,” *Neural Computing & Applications* 35 (2023): 19099–19115, <https://doi.org/10.1007/s00521-023-08740-5>.
43. R. S. Barbosa, J. A. T. Machado, and I. M. Ferreira, “Tuning of PID Controllers Based on Bode’s Ideal Transfer Function,” *Nonlinear Dynamics* 38 (2004): 305–321, <https://doi.org/10.1007/s11071-004-3763-7>.
44. B. Keziz, A. Djouambi, and S. Ladaci, “A New Fractional Order Controller Tuning Method Based on Bode’s Ideal Transfer Function,” *International Journal of Dynamics and Control* 8 (2020): 932–942, <https://doi.org/10.1007/s40435-020-00608-z>.
45. E. Yumuk, M. Güzelkaya, and İ. Eksin, “A Robust Fractional-Order Controller Design With Gain and Phase Margin Specifications Based on Delayed Bode’s Ideal Transfer Function,” *Journal of the Franklin Institute* 359 (2022): 5341–5353, <https://doi.org/10.1016/j.jfranklin.2022.05.033>.
46. D. Izci and S. Ekinci, “A Novel-Enhanced Metaheuristic Algorithm for FOPID-Controlled and Bode’s Ideal Transfer Function–Based Buck Converter System,” *Transactions of the Institute of Measurement and Control* 45 (2023): 1854–1872, <https://doi.org/10.1177/01423312221140671>.

47. R. Pradhan, S. K. Majhi, J. K. Pradhan, and B. B. Pati, "Antlion Optimizer Tuned PID Controller Based on Bode Ideal Transfer Function for Automobile Cruise Control System," *Journal of Industrial Information Integration* 9 (2018): 45–52, <https://doi.org/10.1016/j.jii.2018.01.002>.
48. S. Ekinici, D. Izci, M. Bajaj, and V. Blazek, "Novel Application of Sinh Cosh Optimizer for Robust Controller Design in Hybrid Photovoltaic-Thermal Power Systems," *Scientific Reports* 15 (2025): 2825, <https://doi.org/10.1038/s41598-025-86597-5>.
49. M. Ghasemi, K. Golalipour, M. Zare, et al., "Flood Algorithm (FLA): An Efficient Inspired Meta-Heuristic for Engineering Optimization," *Journal of Supercomputing* 80 (2024): 22913–23017, <https://doi.org/10.1007/s11227-024-06291-7>.
50. H. Su, D. Zhao, A. A. Heidari, et al., "RIME: A Physics-Based Optimization," *Neurocomputing* 532 (2023): 183–214, <https://doi.org/10.1016/j.neucom.2023.02.010>.
51. W. Zhao, L. Wang, and S. Mirjalili, "Artificial Hummingbird Algorithm: A New Bio-Inspired Optimizer With Its Engineering Applications," *Computer Methods in Applied Mechanics and Engineering* 388 (2022): 114194, <https://doi.org/10.1016/j.cma.2021.114194>.
52. D. Izci, S. Ekinici, and A. G. Hussien, "An Elite Approach to Re-Design Aquila Optimizer for Efficient AFR System Control," *PLoS One* 18 (2023): e0291788, <https://doi.org/10.1371/journal.pone.0291788>.
53. S. Ekinici, D. Izci, and M. Kayri, "An Effective Controller Design Approach for Magnetic Levitation System Using Novel Improved Manta Ray Foraging Optimization," *Arabian Journal for Science and Engineering* 47 (2022): 9673–9694, <https://doi.org/10.1007/s13369-021-06321-z>.
54. J. Agarwal, G. Parmar, R. Gupta, and A. Sikander, "Analysis of Grey Wolf Optimizer Based Fractional Order PID Controller in Speed Control of DC Motor," *Microsystem Technologies* 24 (2018): 4997–5006, <https://doi.org/10.1007/s00542-018-3920-4>.
55. S. Ekinici, D. Izci, and M. Yilmaz, "Efficient Speed Control for DC Motors Using Novel Gazelle Simplex Optimizer," *IEEE Access* 11 (2023): 105830–105842, <https://doi.org/10.1109/ACCESS.2023.3319596>.
56. M. Ramezani, D. Bahmanyar, and N. Razmjoo, "A New Improved Model of Marine Predator Algorithm for Optimization Problems," *Arabian Journal for Science and Engineering* 46 (2021): 8803–8826, <https://doi.org/10.1007/s13369-021-05688-3>.
57. D. Izci, "Design and Application of an Optimally Tuned PID Controller for DC Motor Speed Regulation via a Novel Hybrid Lévy Flight Distribution and Nelder–Mead Algorithm," *Transactions of the Institute of Measurement and Control* 43 (2021): 3195–3211, <https://doi.org/10.1177/01423312211019633>.
58. R. M. Rizk-Allah, D. Izci, S. Ekinici, A. Diabat, A. E. Ezugwu, and L. Abualigah, "Incorporating Adaptive Local Search and Experience-Based Perturbed Learning Into Artificial Rabbits Optimizer for Improved DC Motor Speed Regulation," *International Journal of Electrical Power & Energy Systems* 162 (2024): 110266, <https://doi.org/10.1016/j.ijepes.2024.110266>.
59. R. Saini, G. Parmar, and R. Gupta, "An Enhanced Hybrid Stochastic Fractal Search FOPID for Speed Control of DC Motor," in *Fractional Order Systems and Applications in Engineering* (Elsevier, 2023), 51–67, <https://doi.org/10.1016/B978-0-32-390953-2.00011-6>.